# Exploring non-adiabaticity to CO reduction reaction through ab initio molecular dynamics simulation

Fan Zheng and Lin-wang Wang*

*Joint Center for Artificial Photosynthesis and Materials Sciences Division, Lawrence Berkeley National Laboratory, Berkeley, California 94720, USA.*

E-mail: lwwang@lbl.gov

**Abstract**

Non-adiabatic chemical reaction refers to the electronic excitation during reactions. This effect can not be modeled by the ground-state Born-Oppenheimer molecular dynamics (BO-MD), where the electronic structure is at the ground-state for every step of ions' movement. Although the non-adiabatic effect has been explored extensively in gas phase reactions, its role to the electrochemical reactions in electrolyte such as water splitting and $CO_2$ reduction has rarely been explored. On the other hand, electrochemical reactions usually involve electron transport, thus, non-adiabatic process can naturally play a significant role. In this work, using one step of $CO_2$ reduction as an example, we investigate the role of the non-adiabatic effect in the reaction. The reaction barriers are computed by adiabatc BO-MD and non-adiabatic real-time time dependent density functional theory (rt-TDDFT). We find that by including the non-adiabatic effect, rt-TDDFT can increase the reaction barrier up to 6% compared to the BO-MD calculated barrier when solvent model is used to represent the water. Simulations with hybrid solvent model using explicit water molecules around the reaction

site is also carried out under different overpotentials, similar non-adiabatic effects are found.

First-principles methods, such as density function theory (DFT), have been widely used in a variety of electrocatalytical reactions, such as water splitting including oxygen evolution[1–5] and hydrogen evolution reactions,[6–9] $CO_2$ reduction,[10–13] and solar fuel cells.[14–16] By utilizing state-of-art computational techniques such as computational hydrogen electrode model,[17] nudged elastic bands (NEB),[18] and Born-Oppenheimer molecular dynamics (BO-MD),[12] DFT calculations enable a detailed free-energy determination of possible reaction paths, including intermediate states, transition states and reaction barriers. Various effects, for example pH,[19] electrode potential,[10,17] cation induced electric field,[20,21] and electrolyte[12,14,22,23] have been explored systematically to illustrate the reaction mechanisms and to design high-performance catalysis. Most of these methods, particularly to determine the reaction barriers, are based on the ground-state DFT. By assuming a much slower reaction process compared to the time-scale of electron thermalization, the electronic excitations during the related reactions have been ignored, hence, adiabatic Born-Oppenheimer assumption is implicitly used in many studies for electrocatalysis. The non-adiabatic (NA) effect results from the electronic evolution with finite time-scale. However, the NA effect to the electrochemical reactions is rarely explored, and we have very limited knowledge about if the non-adiabaticity will affect the electrochemical reactions and to what extend it can contribute.

Electronic NA effect is defined as the coupling of the electronic ground state to excited eigen-states due to time evolution of the wavefunctions. This effect manifests itself in a chemical reaction when the time-scale of its dynamics is similar to that of the carrier's (electrons and holes) thermalization. As a result, the excited electron (and hole) is not always at its equilibrium ground state. Meanwhile, for non-excited cases with pure charge transport, NA effect can result in charge transfer bottleneck, where carriers need finite time to move from the carrier donor to the acceptor. In comparison, when the reaction is carried out very slowly, the fast relaxation of electronic excitation or fast transfer makes the NA effect unimportant to the reaction. Owing to the ultrafast nature, the NA effect plays a significant

role in chemical reactions such as photochemistry,[24,25] collision,[26] atom-stopping,[26–28] and electron transfer process.[25,29] Particularly, a great deal of research has been focused on gas-phase catalytic reactions on surfaces to understand the contribution from the NA effect.[30–35] For example, the NA simulation with fewest-switches surface-hopping algorithm has shown the strong NA effect for spin flipping and transition during the $O_2$ disssociative adsorption on Al and Pd surface, with the estimated rate consistent to the experiments.[36,37] The reverse process associative desorption of $N_2$ on Ru(001) further shows the NA effect from an *ab initio* simulation indirectly.[38] In that work, consistent agreement between the simulation and the experiments can be obtained only after including the NA effect in the calculation. A comprehensive theoretical study has been made to explore the NA effect of $H_2$/Cu (110) and $N_2$/W (110). However, their simulation has shown a marginal effect of the non-adiabaticity to diatomic molecules adsorption process.[37] Based on these examples, the role of the NA effect seems to depend on specific reaction types. However, for electrochemical reactions under aqueous condition such as heterogenous catalysis, the NA effect has been rarely studied. Electrochemical reactions necessitate the transfer of charge from one place to another, thus it is more likely a NA process. Besides the question of excited state induced by the reaction dynamics, another possibility is the charge transfer bottleneck, which also makes the process NA. One recent work focusing the initial $CO_2$ adsorption to various metal surfaces has shown very fast electronic hybridization compared to the adsorption,[21] showing the adiabatic nature of the chemical adsorption process. Different from the initial adsorption process for $CO_2$ reduction, its subsequent steps involve the proton-assisted electron transfer (PAET). This process also exists in water splitting and hydrogen evolution reactions. Some of the fast PAETs can form the transition state within 1 ps or faster,[39–41] comparable to the time-scale of the electronic thermalization, indicating the potential role of the NA effect. Nonetheless, the NA effect to the electrochemistry reactions with protons addition is rarely investigated in detail. It leaves many questions unanswered: for example, will the NA effect play a role to the electrochemical reactions such as $CO_2$ reduction involving the fast proton motion? If

this is the case, how much does the non-adiabaticity make change to the reaction barrier? Will the NA effect contribute mostly to the carrier excitation or charge transfer bottleneck? How do the electrolyte and applied electrode potential influence the NA?

In this work, we seek to understand the role of the NA effects to heterogenous catalytical reactions in aqueous condition. By using one step of $CO_2$ reduction $\star CO + H_3O^+ + e^- \longrightarrow \star COH + H_2O$ ($\star$: copper surface) on copper [111] surface as an example, we perform the adiabatic (ground-state BO-MD) and non-adiabatic (Erenfest real-time time-dependent DFT (rt-TDDFT)) simulations to model the reaction. In BO-MD, the adiabatic eigen-states are solved by diagonalizing the Hamiltonian at every MD step. The occupation of electrons on each state is based on their eigen-energies. Thus, the electronic structure is always at the ground state for every step. On the contrary, rt-TDDFT evolves the time-dependent wavefunction following Schrödinger's equation, allowing the electronic structure to be excited. Meanwhile, the excitation of the electronic structure may drive the ions movement differently compared to the ground-state electronic structure. With this capability, rt-TDDFT has been widely used to simulate various NA processes such as optical excitations,[42] proton-assisted chemical reactions,[43] and ion sputtering.[27,44] Different from other TDDFT algorithms where a very small time step ($\Delta t$~0.001fs) has to be used to evolve the charge density, the implementation we have adopted here uses the adiabatic states ($\phi_j(t)$) as the basis to expand the wavefunction. These adiabatic states are solved from the Hamiltonian at each ion's step $t_n$ with time-step $\Delta t = t_{n+1} - t_n \leq 0.1$fs. The time-dependent wavefunction is expanded as:

$$\psi_i(t) = \sum_j C_{i,j}(t)\phi_j(t)$$

where adiabatic state $\phi_j(t)$ is solved by diaganolizing the Hamiltonian $H$ at step $t$: $H(t)\phi_j(t) = \epsilon_j(t)\phi_j(t)$. The coefficient $C_{ij}(t)$ for the wavefunction is evolved from $t_n$ to $t_{n+1}$ non-adiabatically following the Schrödinger's equation $i\partial\psi(t)/\partial t = H(t)\psi(t)$ using a much smaller

time-step. The Hamiltonian in the Schrödinger's equation is based on the linear interpolation from $H(t_n)$ to $H(t_{n+1})$. However, since the adiabatic states (size~100) are used as basis to construct the wavefunction and Hamiltonian instead of plane-waves, the evolution of wavefunction from $t_n$ to $t_{n+1}$ involves only a small size matrix, its cost becomes negligible. This method allows us to evolve wavefunction and ions' dynamics of a complex system with hundreds of atoms such as the surface chemical reaction presented here. In this work, the reaction is simulated with CO molecule adsorbed on copper [111] surface, and it is attacked by $H_3O^+$ to form COH on copper. We find that the BO-MD and rt-TDDFT with the same initial setups can reveal opposite results: near the reaction barrier, BO-MD allows the reaction to happen, while rt-TDDFT fails to proceed the reaction to form $\star$COH but return back to $\star$CO. Such difference clearly demonstrates the role of the non-adiabaticity to electrochemical reactions in aqueous conduction. The reaction barrier change caused by the non-adiabaticity is estimated, which is up to 6% correction compared to the ground-state method calculated barriers. We also explored the reaction with the explicit solvent model and with different electrode potentials, and we find similar NA effects.

PWmat[45,46] package based on the plane-wave pseudopotential DFT is used to perform the total energy calculation, structural optimization, BO-MD, and rt-TDDFT. SG15 pseudopotentials[47] with 50 Ryd plane-wave energy cut-off are used to ensure the convergence of charge density. All the structures are relaxed with the forces below 0.02 eV/Å. In our calculation, we choose four-layer Cu[111] slab surface with 3×3 in $x$-$y$ direction superlattice. The most widely used DFT exchange-correlation functionals such as PBE and LDA predict CO adsorption on the hallow site of three Cu atoms, contradicting to the experimentally observed top-site (on top of one Cu atom).[48,49] Instead, we choose revised PBE (revPBE)[50] to reproduce the correct adsorption site. In the dynamical simulations, reaction barrier is sensitive to the length of time step, we find 0.1 fs is enough to obtain accurate reaction barrier (see Supplementary Information (SI)). The rt-TDDFT calculation is also converged with this time step. Both spin-polarized and spin-unpolarized calculations are performed,

but these two types of calculation yield quite similar results.

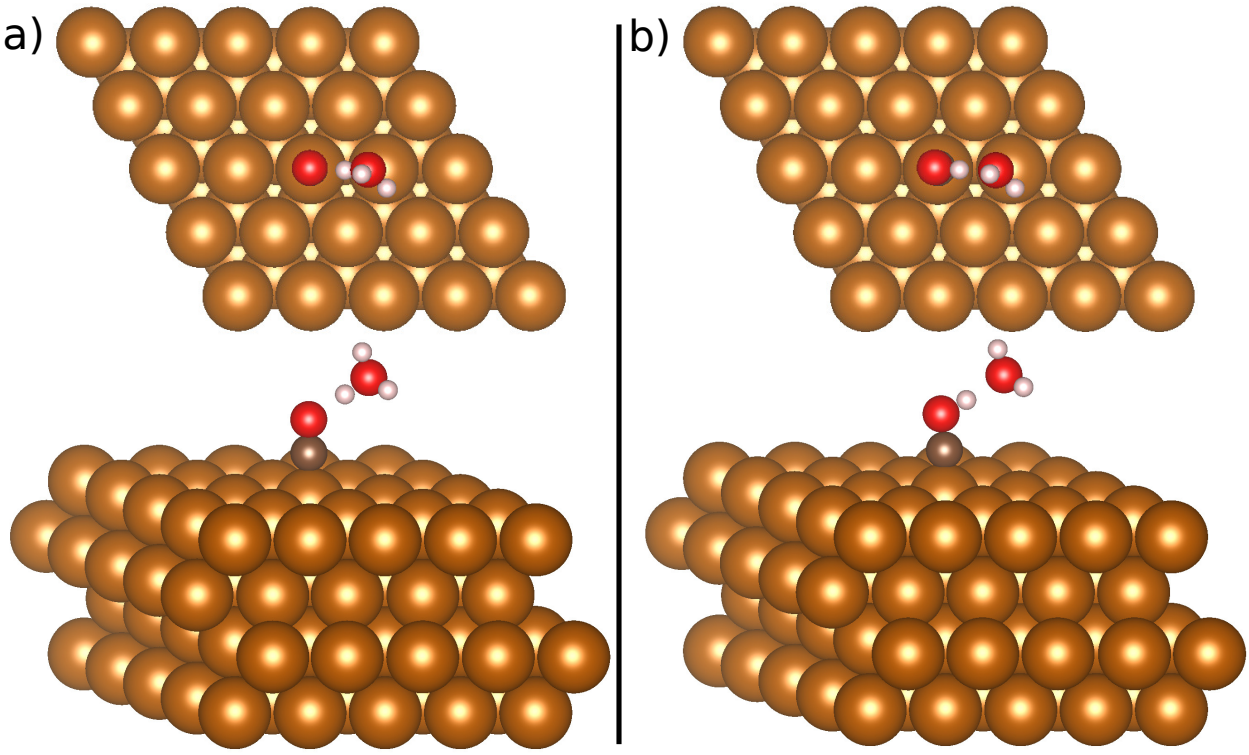


Figure 1: Atomic structures of the a) initial and b) final structures. Top: top view; bottom: side view of the two structures. During the reaction, one proton of hydronium moves from O of $H_3O^+$ to O of $\star$CO. Golden: Cu; Red: O; Brown: C; Light violet: H.

The solvent has been shown to play a significant role in $CO_2$ reduction reactions on metal surfaces. Two types of solvent models are commonly used to represent the solvent effect in DFT calculations: implicit solvent model with continuum dielectric response, and explicit solvent model with water molecules in simulation. In our calculation, we have tried both methods to examine the effect of non-adiabaticity. For the implicit solvent model, when the system contains charged ions such as hydronium with strong solvation energy, the solvent model has to be tuned carefully to yield a correct energy for the ions, so that the energetics of the transition from free hydronium to $\star$COH will be correct. Here, the continuum polarizable solvent model is used with specific ion–solvent interaction parameters.[22,51] The solvent parameters of H and O (belonging to hydronium) are tuned to reproduce the solvation energy of the charged ion. However, computing solvation energy of a charged ion

in water is a non-trivial task due to water fluctuations. Instead, we borrow the idea of the computational hydrogen electrode to compute the free energy of the ion with aqueous condition.[52] Using hydronium as an example, the reaction $H_3O^+(aq) + e^- \longrightarrow \frac{1}{2}H_2(g) + H_2O(aq)$ occurs spontaneously at potential U=0 V. Thus, the enthalpy of $H_3O^+(aq)$ can be expressed as $H(H_3O^+(aq)) = 1/2E(H_2(g)) + E(H_2O(g)) + G_s(H_2O) + 4.44$ eV. Here, $H$ stands for enthalpy, and $G_s(H_2O)$ is the water solvation energy 0.274 eV obtained from the experiment,[53] and 4.44 eV is the hydrogen electrode potential in terms of vacuum. Note, the explicit solvent model is used only to describe the enthalpy, instead of free energy of $H_3O^+(aq)$, in agreement to the early work of implicit solvent model development.[52–54] We tune the solvent parameters of H and O, so that the DFT calculated energy of the hydronium with implicit solvent model matches $H(H_3O^+(aq))$ obtained with the above formula.

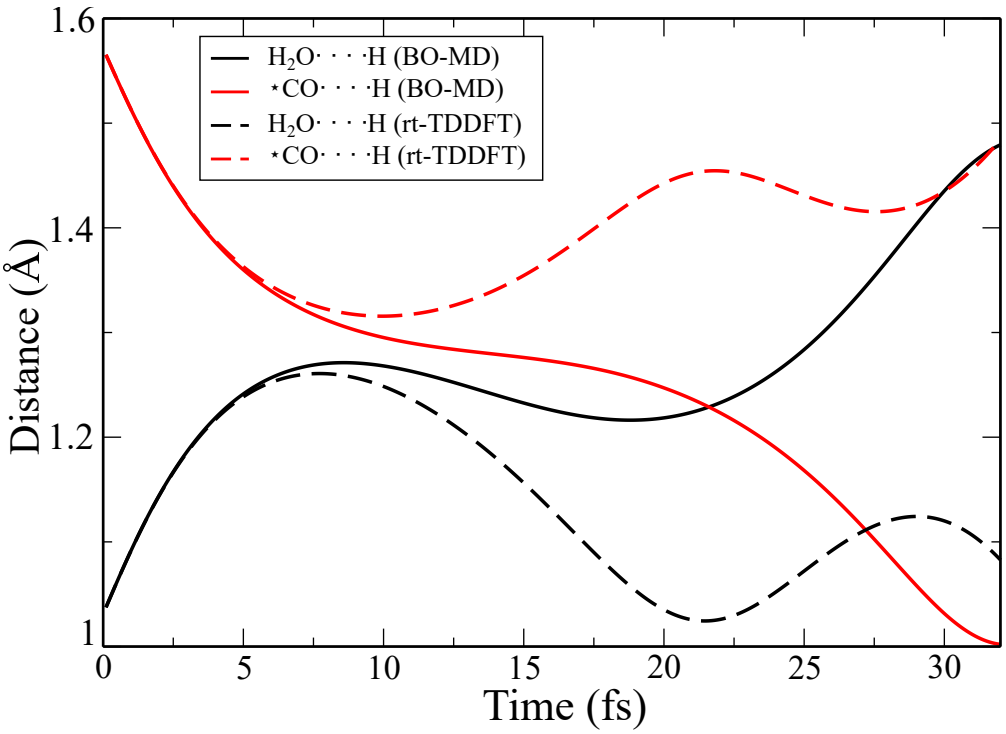


Figure 2: Reaction paths computed by adiabatic BO-MD and NA rt-TDDFT. It records the distance of the proton to oxygen of hydronium and the proton to oxygen of ⋆CO. If the reaction proceeds, the black line and red line switch, indicating the proton transferring from hydronium to ⋆CO. Otherwise, these two lines will return back.

Shown in Fig. 1 is the optimized initial and final structures. The initial structure is built

with hydronium close to $\star$CO with a hydrogen bond, which is a local minimum structure. Such hydrogen bond is optimized yielding a bond length around 1.6 Å. To simulate the reaction with PA-ET using MD, an initial velocity is added to the hydrogen atom of the hydronium close to $\star$CO, with the direction of velocity pointing to the oxygen of $\star$CO. By tuning the magnitude of the initial velocity, we can monitor when the proton can transfer from hydronium to $\star$CO instead of returning. Such initial kinetic energy of the proton can be treated as the reaction barrier. To find the initial atomic configuration and velocity for this reaction to happen at the exact required kinetic energy, we have adopted a "reversed process" procedure. In this procedure, the nudge elastic band (NEB) calculation is performed first to reveal the reaction path and transition state. Then, by starting from the transition-state structure with a very small initial velocities perturbation toward the initial reaction direction, a short BO-MD is performed. This will yield an initial atomic structure. Starting from this atomic position, with reversed velocity, the BO-MD will drive the system to the transition state due to time inversion symmetry. Thus, a slight increase of the initial velocity can lead to a transition to the final state. On the contrary, a slight reduction (e.g. 0.1%) in velocity will prevent the reaction from happening. Using this way, we can quickly identify the adiabatic reaction barrier using BO-MD. For the reaction $\star\mathrm{CO} + \mathrm{H_3O^+} + e^- \longrightarrow \star\mathrm{COH} + \mathrm{H_2O}$, the energy difference $\Delta E = E_{\mathrm{final}} - E_{\mathrm{initial}}$ is calculated to be around 0.5 eV. In the experiment, an overpotential is added to overcome $\Delta E$ or to make it negative to make the reaction to proceed spontaneous. To mimic the applied overpotential to the electrode, we add two electrons to the system and relax the structures so that the energy difference between the initial and final structures is close to zero. Fig. 2 shows the reaction paths computed with BO-MD and rt-TDDFT. In this figure, both calculations of BO-MD and rt-TDDFT start from the same initial structures and velocities as well as initial electronic structure. The initial kinetic energy of the proton equals the BO-MD reaction barrier to just let the reaction happen. For BO-MD simulation, the proton of hydronium move from $\mathrm{H_3O^+}$ to $\star$CO quickly at the beginning. Then it starts to slow down from 10 fs to 25 fs. Eventually it

bonds to ⋆CO after around 30 fs indicated by the exchange of the distances toward CO and $H_2O$. We extend the simulation up to 70 fs to make sure the proton will not return back to water molecule. However, rt-TDDFT reveals a completely different reaction path. The proton follows almost the same reaction path of BO-MD at the beginning. But it deviates with the BO-MD's path after around 5 fs, proceeding to the opposite results in the end. During the simulation, the proton does not move across the reaction barrier, but it returns back to water molecules re-forming the initial structure. We also perform rt-TDDFT up to 70 fs to confirm that the reaction does not happen during this time.

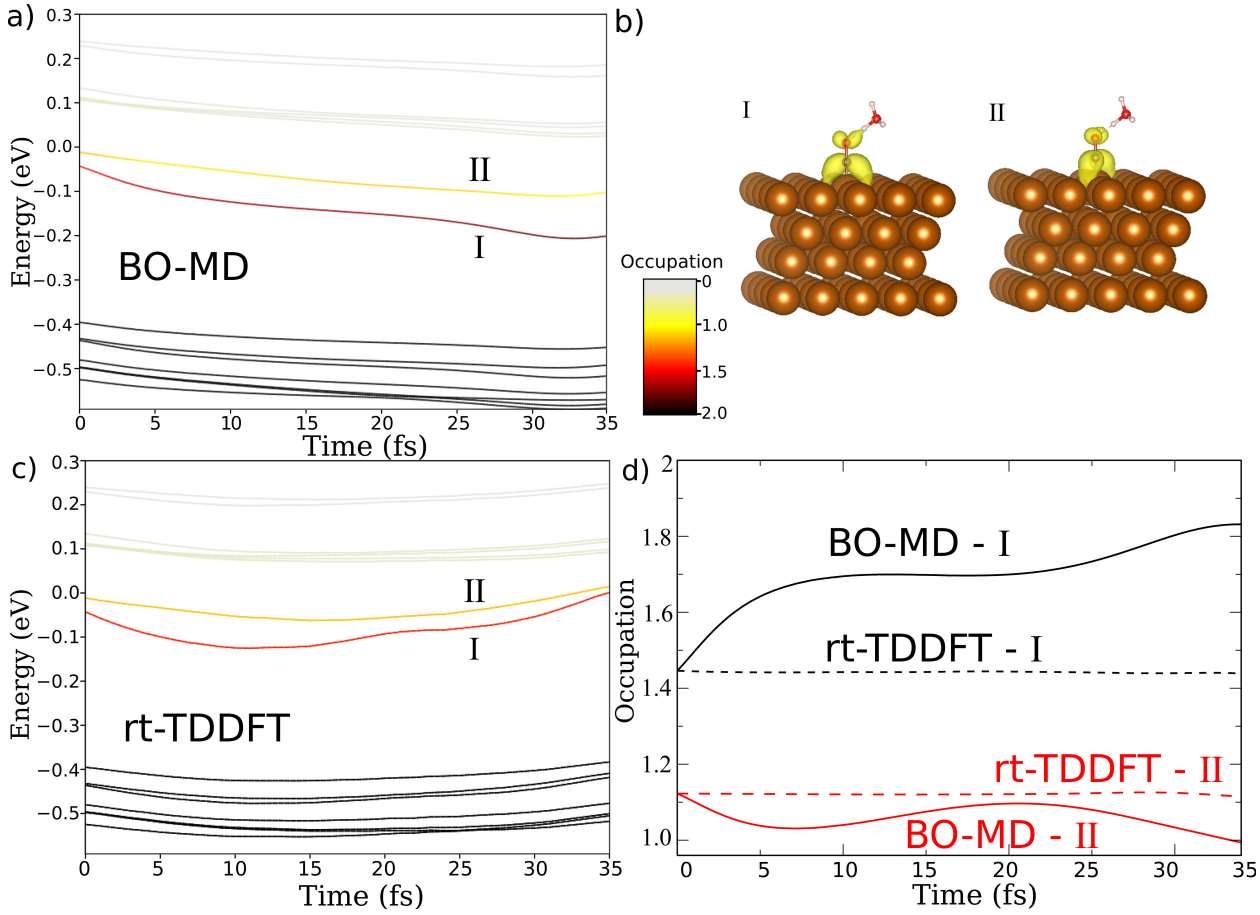


Figure 3: a) Eigen energies and occupations of the states near Fermi energy, extracted from BO-MD simulation. b) I: Charge density of the state at time $t$=0 fs with eigen energy around -0.01 eV. Its initial occupation is 1.1. II: Charge density for the state with eigen-energy around -0.04 eV at $t$=0 fs. It initial occupation is around 1.45. c) Eigen-energies and occupations of the states near Fermi energy, extracted from rt-TDDFT simulation with the same initial structure and velocity to BO-MD. d) Occupations of the adiabatic state (I and II) as a function of time for BO-MD and rt-TDDFT simulations.

To unveil the underlying reason for the dramatic difference, Fig. 3a shows the eigenenergies for the states near the Fermi level in BO-MD simulation. The colors indicate the occupation of the states during the reaction. Near the Fermi level, there are two eigenstates with wavefunctions mostly on adsorbed CO on copper as shown in Fig. 3b. At time $t$ = 0 fs, these two states are almost degenerate except that they are splitted owing to the weak hybridization with $H_3O^+$. During the reaction (Fig. 3a), most of the states have relatively small changes, except the state hybridized with hydronium near Fermi level. When the proton is moving close to $\star$CO, the energy of state I becomes lower, indicating the hybridization developed between the proton and $\star$CO. More importantly, we also track the change of the occupation of this state as shown in Fig. 3d. Initially, at $t$ = 0 and room temperature, the state I is 72% occupied, while the state II is 55% occupied. As the reaction goes, the occupation of state I rises until it is fully occupied. On the other hand, the occupation of state II slightly reduces. The total occupation of 2.55 increases to about 3.0 (non-spin case). Thus, there are around 0.45 electrons increase on these two levels. Such 0.45 electrons increase indicates that the previously empty proton is occupied by electrons. Enough charge occupation on H manifests the bond formation between H and CO. The major part of the 0.45 electron transfer is provided from Cu slab. Such electron transfer from Cu can be verified by a direct charge measurement before and after the reaction. With a horizontal plane ($x-y$ plane) with its $z$-value in the middle between the top-layer Cu and C atoms, the total electrons above this plane is found to increase by 0.35 after the reaction. This is also consistent with the results reported in Ref. 21. It is interesting that this charge is not 1. Under the computational hydrogen electrode (CHE) approximation, this charge transfer should be 1.

The above picture is dramatically different in rt-TDDFT simulation. As shown in Fig. 3c, at the beginning of the reaction, the state I and II change in similar way as in the BO-MD. But after 15 fs, they become different. More dramatically, the occupations of state I and II almost do not change during the simulation time. The occupation on the adiabatic state I

and II are calculated as: $f_j(t) = \sum_i |\langle\phi_j(t)|\,\psi_i(t)\rangle|^2\, O(i) = \sum_i |C_{i,j}(t)|^2\, O(i)$, where $O(i)$ is the occupation of the time evolution wavefunction $\psi_i(t)$ which does not change under rt-TDDFT. The charge on H is controlled by both the hybridization strength of the adiabatic CO-H state and the occupation for this state. If starting the simulation from same initial structure and velocities to BO-MD, the relative constant $f_j(t)$ for state I and II by rt-TDDFT leads to the situation that less charge is transferred to H from Cu, which suppresses the proton's motion towards CO and reduces the bond strength of CO-H bond eventually. As a result, there is no formation of CO-H bond (due to the lack of electrons), and the system bounces back to $H_3O^+$ as shown in Fig. 2. The lack of charge transfer is also verified by the direct charge measurement above the horizontal plane as discussed above. The change of charge from Cu is less than 0.35 compared to BO-MD (Fig. 4b). This example clearly shows how the non-adiabaticity plays a role in electrochemical reactions. Although this is only for one step, the observation is general since most of the reduction and oxidation reactions involves fast protonation or deprotonation.

For the rt-TDDFT simulation, the microscopic mechanism for the reaction becomes quite different from that of BO-MD. In order to induce the reaction, a higher initial velocity shall be provided. In this case, we find that at least 12 meV additional initial kinetic energy must be supplied, corresponding to 6.1% reaction barrier underestimation by BO-MD and other ground-state calculation methods. It is interesting to investigate how the reaction can happen if the occupations of adiabatic states tend to be constant. Shown in Fig. 4a compares two simulations (BO-MD and rt-TDDFT) with both giving rise to the reactions by just overcoming the barrier (thus rt-TDDFT has higher initial velocities than BO-MD). Similar to the above rt-TDDFT case which has the same velocities to BO-MD, the occupations of the state I and II in this rt-TDDFT simulation are mostly unchanged starting from $t = 0$ fs. However, for a given time during the reaction, the proton is closer to CO than that of BO-MD, owing to its higher initial velocity in TDDFT. Although the occupations of the adiabatic state I and II are constant, the adiabatic CO-H hybridization is stronger in rt-TDDFT because

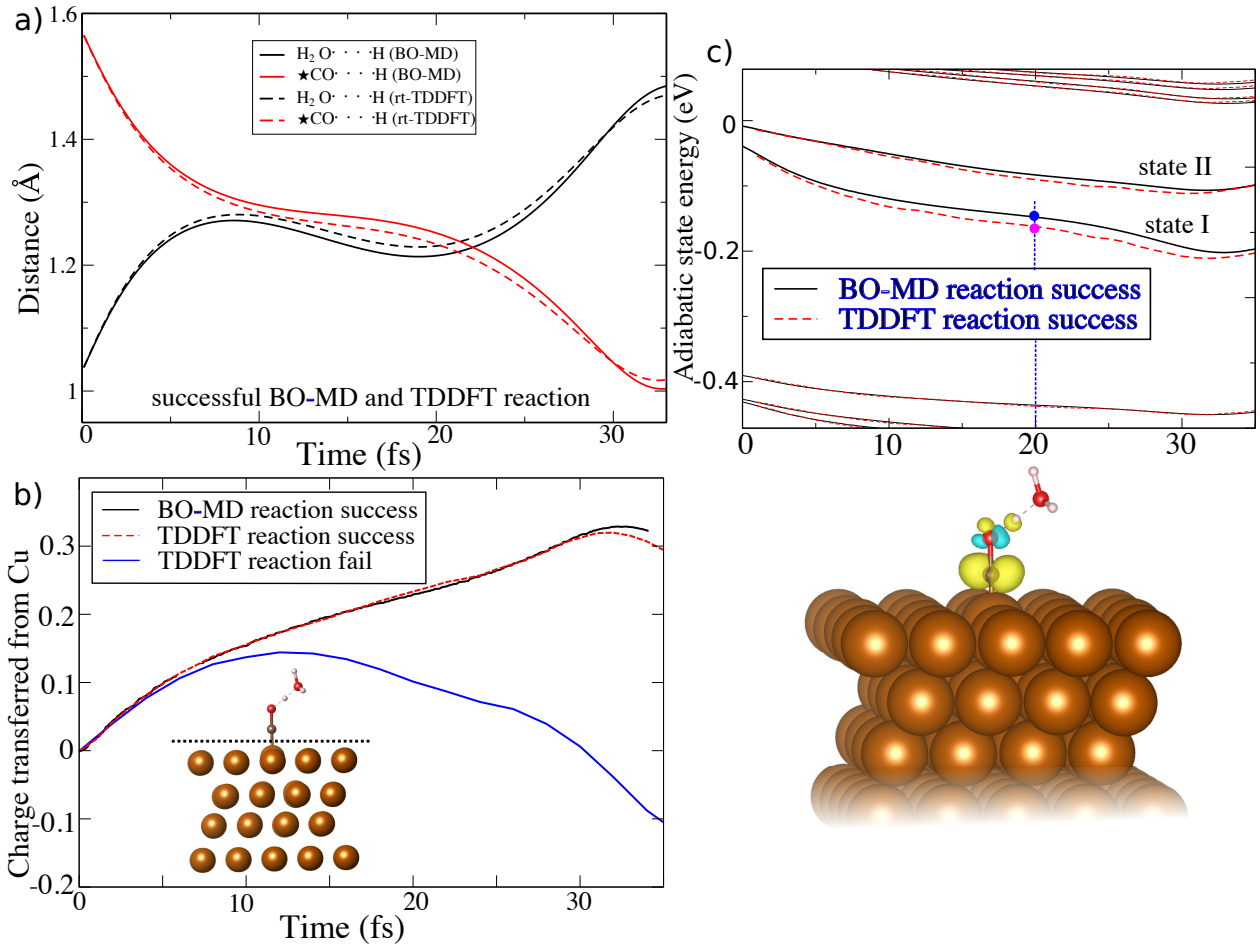


Figure 4: a) Reaction paths for BO-MD and rt-TDDFT. Both simulations have proton bonding to ⋆CO to make the reaction successful (thus rt-TDDFT has a higher initial velocity than BO-MD). b) Measured change of total charge counted above the plane. This horizontal plane has its $z$-value in the middle between C and top Cu layer. Here, simulation-"TDDFT reaction fail" has the same initial velocity to "BO-MD reaction success", while "TDDFT reaction success" has higher initial velocity than "BO-MD reaction success". c) Eigen-energy of the adiabatic states for "BO-MD reaction success" and "TDDFT reaction success". The bottom isosurface is the state I charge density difference of BO-MD and rt-TDDFT at $t$ = 20 fs (charge density at "Red" dot minus "Blue" dot). Yellow color in the isosurface indicates positive; blue indicates negative.

of the closer distance between H and CO. This can be shown in Fig. 4c, where the charge density difference of the adiabatic state I from TDDFT and BO-MD at 20 fs is plotted as an example. It shows the electron gain near the proton for the adiabatic state I in rt-TDDFT. Such stronger hybridization between CO and H compensates for the invariant occupation in rt-TDDFT, transferring enough charge to the proton to form the CO-H bond and finish the reaction. Meanwhile, the change of charge above Cu substrate is measured during this rt-TDDFT simulation (Fig. 4b). Compared to BO-MD, rt-TDDFT (reaction success) shows quite similar change of the charge out of Cu, and rt-TDDFT (reaction success) does not show a slower charge transfer. Thus, we believe the charge transfer bottleneck is a less dominant consequence of NA effect.

Finally, we examine the situation with spin-polarization. After turning on the spin, the reaction path shows negligible difference compared to Fig. 2. We do note that, if the $k$-point is not sufficient, in some cases, for the BO-MD simulation, after the proton exchange, the system can become spin-polarized. We expect this could be a real case if CO is sitting in small Cu cluster instead of bulk Cu (see SI Fig. 4). This spin-polarization however, will never be developed in rt-TDDFT, since such spin flip is impossible without spin-orbit coupling. Even with spin-orbit, the time of the reaction discussed here will not be enough to make such spin flip.

As afore discussed, the implicit solvent model reproduces the energetic of the solvation effect to ions. However, it does has its disadvantages,[55] primarily as an averaged continuum media, it lacks the atomistic bonding information. More importantly, for dynamical simulations, implicit solvent has instant dielectric screening response. But in reality, the surrounding water will not have enough time to rotate itself and re-arrange the structure following the fast proton transfer movement. Meanwhile, the surrounding water molecules could form hydrogen bonds with hydronium or even with $\star$CO to change the energy levels. To overcome this challenge, we utilize a hybrid solvent model by sampling an explicit water molecules layer around the reaction site. Implicit solvent model is still used outside

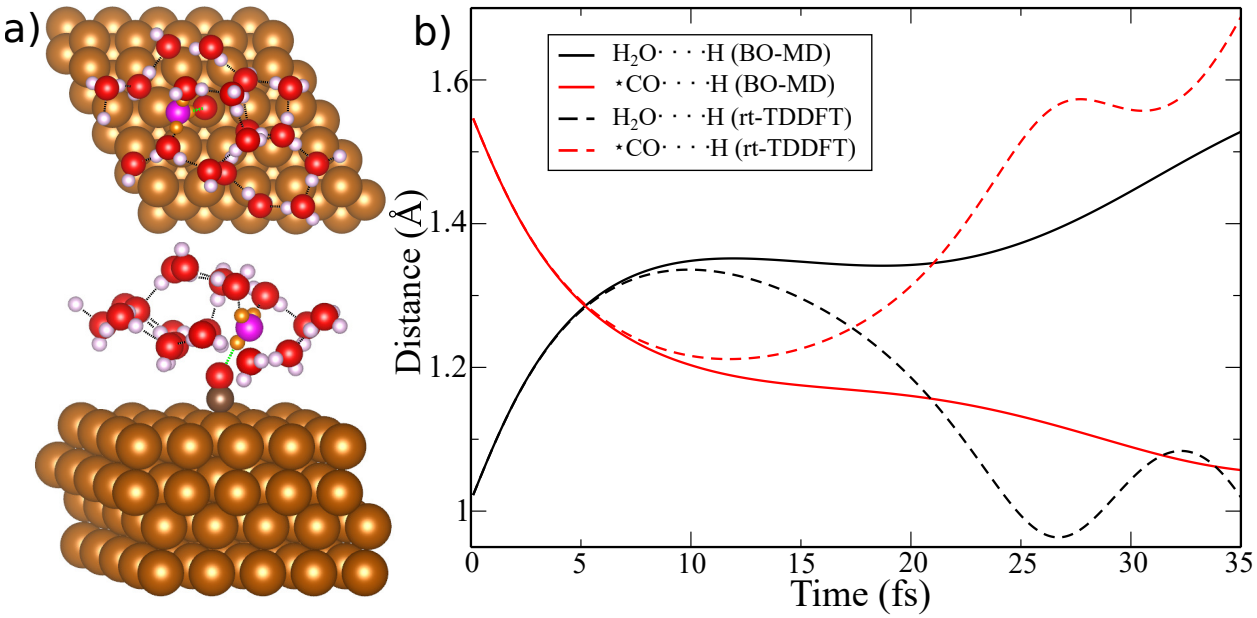


Figure 5: a) Structure of Cu/CO/H3O$^+$ with additional 14 $H_2O$ molecules around reaction site. Top: Top view, Botom: side view. Black and green dashed lines are hydrogen bonds between water molecules, hydrogen bonds between hydronium and $\star$CO, respectively. Hydronium are highlighted with different colors (Violet: oxygen, Orange: Hydrogen) for clarity. b) Reaction paths simulated by BO-MD and rt-TDDFT with same initial structures and velocities.Similar to Fig. 2, it records the distance of the proton to oxygen of hydronium and the proton to oxygen of $\star$CO.

the explicit solvent model layer. Obtaining the structure for the water molecules is not trivial. Here, the in-house code based on the genetic algorithm is used to find the global energy-minimum (see SI). Genetic-algorithm structure searching is analogous to the evolutionary process in the biology. For a population consisting of finite number of structures, the structures with lower free energies are more likely to be selected to combine into the child generation, similar to the nature selection. By iterating such selection process from the parent- to child-generation, it is possible to find out the global minimum given enough number of generations. In this case, we add another 14 water molecules around $\star$CO and hydronium. $\star$CO and hydronium are fixed during the evolutionary iterations (see SI). Shown in Fig. 5a is the final structure obtained. To make the free energies of the initial and final structures to be the same, 4 additional electrons are added to the system. Following the same procedure for the implicit solvent model case, we perform ground-state NEB to find the reaction path, reverse and tune the velocities to get BO-MD reaction barrier. Here, the BO-MD or NEB calculated adiabatic barrier is higher than those with implicit solvent. This is becuase at the transition state where the proton is in the middle of CO and $H_2O$, there is a strong solvent polarization energy towards the relatively isolated proton in the implicit model case. Such polarization energy does not exist in the explicit water molecule due to the lack of response of the surrounding water molecules. rt-TDDFT is carried out with the same initial condition that is used for BO-MD. However, the NA effect becomes important near the reaction barrier similar to the implicit solvent case: rt-TDDFT and BO-MD yield opposite results for the reaction as shown in Fig. 5b. The electronic structure's evolution by BO-MD is illustrated in SI Fig.5, including their occupations. As the reaction goes, the eigen-energy of the state is lowered indicating the development of the hybridization between the proton and $\star$CO. Meanwhile, BO-MD predicts the increased occupation of this state. But rt-TDDFT illustrates a constant value for the occupations (shown in SI Fig.5c), although the energies of the adiabatic states is lowered owing to the hybridization. Eventually, the reaction does not happen and it returns back to the initial structure.

Here, the number of added electrons is to mimic the applied overpotential. Meantime, we perform the calculation with 3 additional electrons. In this case, reducing one electron shifts up the relative free energy of the final ⋆COH structure by around 0.2 eV. The calculated ground-state barrier is increased from 0.36 eV to 0.41 eV. Using BO-MD and rt-TDDFT, the reaction paths and the evolutions of the electronic structure including occupations are shown in SI SFig.6. These results indicate clearly that the NA effect still plays a role when the applied potential is altered. We also perform both spin-polarized and spin-unpolarized calculations. These two types of calculation give almost the same reaction path and eigen-energy/occupation change during the reaction, i.e. the system is always non-magnetic during the reaction. Table. 1 lists the reaction barrier calculated by the adiabatic methods and rt-TDDFT involving the non-adiabaticity. From Table. 1, we see that although the three cases (implicit solvent, explicit solvent model and different overpotential) have rather different barrier, the barrier increase due to NA effect are all similar around 10 meV.

Table 1: Reaction barriers calculated by NEB, BO-MD and rt-TDDFT. Here, NEB and BO-MD are only ground-state calculations. rt-TDDFT involves the NA effect beyond the ground-state approximation. Last column is the percentage change of the barrier by the NA effect.

| Reaction Barrier $E$ | $E_{\mathrm{NEB}}$ (eV) | $E_{\mathrm{BO-MD}}$ (eV) | $E_{\mathrm{rt-TDDFT}}$ (eV) | $E_{\mathrm{rt-TDDFT}} - E_{\mathrm{BO-MD}}$ (meV) |
|---|---|---|---|---|
| Implicit solvent (add $2e^-$) | 0.080 | 0.196 | 0.208 | 12 |
| Hybrid solvent (add $4e^-$) | 0.360 | 0.288 | 0.299 | 11 |
| Hybrid solvent (add $3e^-$) | 0.411 | 0.363 | 0.373 | 10 |

To summarize, using one step of $CO_2$ reduction on copper [111] surface ($\star CO + H_3O^+ + e^- \longrightarrow \star COH + H_2O$) as an example, we investigate how the NA effect is involved to influence the reaction. We believe this is one of the first few works to directly illuminate the NA effect in electrochemical reaction with the electrolytes. In this reaction, the proton of hydronium is attacking ⋆CO to form ⋆COH. By tuning initial velocity of the proton and monitoring the reaction using ground-state BO-MD, we can identify the adiabatic reaction barrier to be the initial kinetic energy of the proton, which just let the reaction to finish. However, by using the same initial kinetic energy and structure, although BO-MD can finish

the reaction, rt-TDDFT simulation involving the NA effect disallow the reaction to finish but return the proton back to hydronium. A higher kinetic energy must be supplied to drive the proton move over the barrier to form the final structure. Additional electrons are added to the system to mimic the applied overpotential to the electrode. Both implicit continuum solvent and explicit water solvent are used to simulate the same reaction. However, the NA effect still remains in all the case. Our calculation demonstrates that involving the NA effect increases the reaction barrier by 10 meV for all the models and electrode potentials we have tested.

# Acknowledgement

This material is based on the work performed by the Joint Center for Artificial Photosynthesis, a DOE Energy Innovation Hub, supported through the Office of Science of the U.S. Department of Energy under Award number DE-SC0004993. We use the resource of National Energy Research Scientific Computing center (NERSC) located in Lawrence Berkeley National Laboratory and the computational resource of the Oak Ridge Leadership Computing Facility at the Oak Ridge National Laboratory under the Innovative and Novel Computational Impact on Theory and Experiment project.

# References

(1) Valdés, Á.; Qu, Z.-W.; Kroes, G.-J.; Rossmeisl, J.; Nørskov, J. K. Oxidation and Photo-Oxidation of Water on TiO2 Surface. *The Journal of Physical Chemistry C* **2008**, *112*, 9872–9879.

(2) Pham, T. A.; Ping, Y.; Galli, G. Modelling Heterogeneous Interfaces for Solar Water Splitting. *Nature Materials* **2017**, *16*, 401–408.

(3) Pham, H. H.; Cheng, M.-J.; Frei, H.; Wang, L.-W. Surface Proton Hopping and Fast-

Kinetics Pathway of Water Oxidation on Co $_3$ O $_4$ (001) Surface. *ACS Catalysis* **2016**, *6*, 5610–5617.

(4) Wu, Y.; Lazic, P.; Hautier, G.; Persson, K.; Ceder, G. First Principles High Throughput Screening of Oxynitrides for Water-Splitting Photocatalysts. *Energy & Environmental Science* **2013**, *6*, 157–168.

(5) Zhou, Y.; Gao, G.; Li, Y.; Chu, W.; Wang, L.-W. Transition-Metal Single Atoms in Nitrogen-Doped Graphenes as Efficient Active Centers for Water Splitting: A Theoretical Study. *Physical Chemistry Chemical Physics* **2019**, *21*, 3024–3032.

(6) Greeley, J.; Jaramillo, T. F.; Bonde, J.; Chorkendorff, I.; Nørskov, J. K. Computational High-Throughput Screening of Electrocatalytic Materials for Hydrogen Evolution. *Nature Materials* **2006**, *5*, 909–913.

(7) Chhetri, M.; Maitra, S.; Chakraborty, H.; V. Waghmare, U.; R. Rao, C. N. Superior Performance of Borocarbonitrides, B x C y N z , as Stable, Low-Cost Metal-Free Electrocatalysts for the Hydrogen Evolution Reaction. *Energy & Environmental Science* **2016**, *9*, 95–101.

(8) Tang, Q.; Jiang, D.-e. Mechanism of Hydrogen Evolution Reaction on 1T-MoS2 from First Principles. *ACS Catalysis* **2016**, *6*, 4953–4961.

(9) Gao, G.; O'Mullane, A. P.; Du, A. 2D MXenes: A New Family of Promising Catalysts for the Hydrogen Evolution Reaction. *ACS Catalysis* **2017**, *7*, 494–500.

(10) A. Peterson, A.; Abild-Pedersen, F.; Studt, F.; Rossmeisl, J.; K. Nørskov, J. How Copper Catalyzes the Electroreduction of Carbon Dioxide into Hydrocarbon Fuels. *Energy & Environmental Science* **2010**, *3*, 1311–1315.

(11) Montoya, J. H.; Peterson, A. A.; Nørskov, J. K. Insights into C-C Coupling in CO2 Electroreduction on Copper Electrodes. *ChemCatChem* **2013**, *5*, 737–742.

(12) Cheng, T.; Xiao, H.; Goddard, W. A. Free-Energy Barriers and Reaction Mechanisms for the Electrochemical Reduction of CO on the Cu(100) Surface, Including Multiple Layers of Explicit Solvent at pH 0. *The Journal of Physical Chemistry Letters* **2015**, *6*, 4767–4773.

(13) Cheng, T.; Xiao, H.; Goddard, W. A. Reaction Mechanisms for the Electrochemical Reduction of CO2 to CO and Formate on the Cu(100) Surface at 298 K from Quantum Mechanics Free Energy Calculations with Explicit Water. *Journal of the American Chemical Society* **2016**, *138*, 13802–13805.

(14) Ping, Y.; Goddard, W. A.; Galli, G. A. Energetics and Solvation Effects at the Photoanode/Catalyst Interface: Ohmic Contact versus Schottky Barrier. *Journal of the American Chemical Society* **2015**, *137*, 5264–5267.

(15) Scheuermann, A. G.; Lawrence, J. P.; Kemp, K. W.; Ito, T.; Walsh, A.; Chidsey, C. E. D.; Hurley, P. K.; McIntyre, P. C. Design Principles for Maximizing Photovoltage in Metal-Oxide-Protected Water-Splitting Photoanodes. *Nature Materials* **2016**, *15*, 99–105.

(16) Yan, Q.; Yu, J.; Suram, S. K.; Zhou, L.; Shinde, A.; Newhouse, P. F.; Chen, W.; Li, G.; Persson, K. A.; Gregoire, J. M.; Neaton, J. B. Solar Fuels Photoanode Materials Discovery by Integrating High-Throughput Theory and Experiment. *Proceedings of the National Academy of Sciences* **2017**, *114*, 3040–3043.

(17) Nørskov, J. K.; Rossmeisl, J.; Logadottir, A.; Lindqvist, L.; Kitchin, J. R.; Bligaard, T.; Jónsson, H. Origin of the Overpotential for Oxygen Reduction at a Fuel-Cell Cathode. *The Journal of Physical Chemistry B* **2004**, *108*, 17886–17892.

(18) Berne, B. J.; Ciccotti, G.; Coker, D. F. [No Title Found]. Classical and Quantum Dynamics in Condensed Phase Simulations. LERICI, Villa Marigola, 1998.

(19) Rossmeisl, J.; Chan, K.; Ahmed, R.; Tripković, V.; E. Björketun, M. pH in Atomic Scale Simulations of Electrochemical Interfaces. *Physical Chemistry Chemical Physics* **2013**, *15*, 10321–10325.

(20) Ringe, S.; Clark, E. L.; Resasco, J.; Walton, A.; Seger, B.; Bell, A. T.; Chan, K. Understanding Cation Effects in Electrochemical CO2 Reduction. *Energy & Environmental Science* **2019**, *12*, 3001–3014.

(21) Bajdich, M.; Fields, M.; Chen, L. D.; Sandberg, R. B.; Chan, K.; Nørskov, J. K. Electron Transfer to CO2 during Adsorption at the Metal — Solution Interface.

(22) Andreussi, O.; Dabo, I.; Marzari, N. Revised Self-Consistent Continuum Solvation in Electronic-Structure Calculations. *The Journal of Chemical Physics* **2012**, *136*, 064102.

(23) Mathew, K.; Sundararaman, R.; Letchworth-Weaver, K.; Arias, T. A.; Hennig, R. G. Implicit Solvation Model for Density-Functional Study of Nanocrystal Surfaces and Reaction Pathways. *The Journal of Chemical Physics* **2014**, *140*, 084106.

(24) Tritsaris, G. A.; Vinichenko, D.; Kolesov, G.; Friend, C. M.; Kaxiras, E. Dynamics of the Photogenerated Hole at the Rutile TiO2(110)/Water Interface: A Nonadiabatic Simulation Study. *The Journal of Physical Chemistry C* **2014**, *118*, 27393–27401.

(25) Hammes-Schiffer, S. Theory of Proton-Coupled Electron Transfer in Energy Conversion Processes. *Accounts of chemical research* **2009**, *42*, 1881–1889.

(26) Wang, Z.; Li, S.-S.; Wang, L.-W. Efficient Real-Time Time-Dependent Density Functional Theory Method and Its Application to a Collision of an Ion with a 2D Material. *Physical Review Letters* **2015**, *114*.

(27) Bi, G.; Kang, J.; Wang, L.-W. High Velocity Proton Collision with Liquid Lithium: A Time Dependent Density Functional Theory Study. *Physical Chemistry Chemical Physics* **2017**, *19*, 9053–9058.

(28) Yost, D. C.; Yao, Y.; Kanai, Y. Examining Real-Time Time-Dependent Density Functional Theory Nonequilibrium Simulations for the Calculation of Electronic Stopping Power. *Physical Review B* **2017**, *96*.

(29) Wang, D.; Liu, Z.-P.; Yang, W.-M. Proton-Promoted Electron Transfer in Photocatalysis: Key Step for Photocatalytic Hydrogen Evolution on Metal/Titania Composites. *ACS Catalysis* **2017**, *7*, 2744–2752.

(30) Alducin, M.; Díez Muiño, R.; Juaristi, J. Non-Adiabatic Effects in Elementary Reaction Processes at Metal Surfaces. *Progress in Surface Science* **2017**, *92*, 317–340.

(31) Kroes, G.-J.; Juaristi, J. I.; Alducin, M. Vibrational Excitation of H2 Scattering from Cu(111): Effects of Surface Temperature and of Allowing Energy Exchange with the Surface. *The Journal of Physical Chemistry C* **2017**, *121*, 13617–13633.

(32) Jiang, B.; Alducin, M.; Guo, H. Electron–Hole Pair Effects in Polyatomic Dissociative Chemisorption: Water on Ni(111). *The Journal of Physical Chemistry Letters* **2016**, *7*, 327–331.

(33) Luo, X.; Jiang, B.; Juaristi, J. I.; Alducin, M.; Guo, H. Electron-Hole Pair Effects in Methane Dissociative Chemisorption on Ni(111). *The Journal of Chemical Physics* **2016**, *145*, 044704.

(34) Füchsel, G.; del Cueto, M.; Díaz, C.; Kroes, G.-J. Enigmatic HCl + Au(111) Reaction: A Puzzle for Theory and Experiment. *The Journal of Physical Chemistry C* **2016**, *120*, 25760–25779.

(35) Goikoetxea, I.; Juaristi, J. I.; Alducin, M.; Muiño, R. D. Dissipative Effects in the Dynamics of N2on Tungsten Surfaces. *Journal of Physics: Condensed Matter* **2009**, *21*, 264007.

(36) Carbogno, C.; Behler, J.; Reuter, K.; Groß, A. Signatures of Nonadiabatic ${\text{O}}_{2}$ Dissociation at Al(111): First-Principles Fewest-Switches Study. *Physical Review B* **2010**, *81*, 035410.

(37) Juaristi, J. I.; Alducin, M.; Muiño, R. D.; Busnengo, H. F.; Salin, A. Role of Electron-Hole Pair Excitations in the Dissociative Adsorption of Diatomic Molecules on Metal Surfaces. *Physical Review Letters* **2008**, *100*, 116102.

(38) Diekhöner, L.; Hornekær, L.; Mortensen, H.; Jensen, E.; Baurichter, A.; Petrunin, V. V.; Luntz, A. C. Indirect Evidence for Strong Nonadiabatic Coupling in N2 Associative Desorption from and Dissociative Adsorption on Ru(0001). *The Journal of Chemical Physics* **2002**, *117*, 5018–5030.

(39) Fischer, S. A.; Duncan, W. R.; Prezhdo, O. V. Ab Initio Nonadiabatic Molecular Dynamics of Wet-Electrons on the TiO2 Surface. *Journal of the American Chemical Society* **2009**, *131*, 15483–15491.

(40) Petek, H.; Zhao, J. Ultrafast Interfacial Proton-Coupled Electron Transfer. *Chemical Reviews* **2010**, *110*, 7082–7099.

(41) Oscar, B. G.; Liu, W.; Rozanov, N. D.; Fang, C. Ultrafast Intermolecular Proton Transfer to a Proton Scavenger in an Organic Solvent. *Physical Chemistry Chemical Physics* **2016**, *18*, 26151–26160.

(42) Turro, N. J. *Modern Molecular Photochemistry*; University Science Books, 1991.

(43) Hammes-Schiffer, S. Theoretical Perspectives on Proton-Coupled Electron Transfer Reactions. *Accounts of Chemical Research* **2001**, *34*, 273–281.

(44) Miyamoto, Y.; Zhang, H. Electronic Excitation in an ${\mathrm{Ar}}^{7+}$ Ion Traversing a Graphene Sheet: Molecular Dynamics Simulations. *Physical Review B* **2008**, *77*, 161402.

(45) Jia, W.; Cao, Z.; Wang, L.; Fu, J.; Chi, X.; Gao, W.; Wang, L.-W. The Analysis of a Plane Wave Pseudopotential Density Functional Theory Code on a GPU Machine. *Computer Physics Communications* **2013**, *184*, 9–18.

(46) Jia, W.; Fu, J.; Cao, Z.; Wang, L.; Chi, X.; Gao, W.; Wang, L.-W. Fast Plane Wave Density Functional Theory Molecular Dynamics Calculations on Multi-GPU Machines. *Journal of Computational Physics* **2013**, *251*, 102–115.

(47) Hamann, D. R. Optimized Norm-Conserving Vanderbilt Pseudopotentials. *Physical Review B* **2013**, *88*, 085117.

(48) Kresse, G.; Gil, A.; Sautet, P. Significance of Single-Electron Energies for the Description of CO on Pt(111). *Physical Review B* **2003**, *68*.

(49) Mason, S. E.; Grinberg, I.; Rappe, A. M. First-Principles Extrapolation Method for Accurate CO Adsorption Energies on Metal Surfaces. *Physical Review B* **2004**, *69*.

(50) Hammer, B.; Hansen, L. B.; Nørskov, J. K. Improved Adsorption Energetics within Density-Functional Theory Using Revised Perdew-Burke-Ernzerhof Functionals. *Physical Review B* **1999**, *59*, 7413–7421.

(51) Mathew, K.; Sundararaman, R.; Letchworth-Weaver, K.; Arias, T. A.; Hennig, R. G. Implicit Solvation Model for Density-Functional Study of Nanocrystal Surfaces and Reaction Pathways. *The Journal of Chemical Physics* **2014**, *140*, 084106.

(52) Bryantsev, V. S.; Diallo, M. S.; Goddard III, W. A. Calculation of Solvation Free Energies of Charged Solutes Using Mixed Cluster/Continuum Models. *The Journal of Physical Chemistry B* **2008**, *112*, 9709–9719.

(53) Zhan, C.-G.; Dixon, D. A. First-Principles Determination of the Absolute Hydration Free Energy of the Hydroxide Ion. *The Journal of Physical Chemistry A* **2002**, *106*, 9737–9744.

(54) Palascak, M. W.; Shields, G. C. Accurate Experimental Values for the Free Energies of Hydration of H+, OH-, and H3O+. *The Journal of Physical Chemistry A* **2004**, *108*, 3692–3694.

(55) Gauthier, J. A.; Ringe, S.; Dickens, C. F.; Garza, A. J.; Bell, A. T.; Head-Gordon, M.; Nørskov, J. K.; Chan, K. Challenges in Modeling Electrochemical Reaction Energetics with Polarizable Continuum Models. *ACS Catalysis* **2019**, *9*, 920–931.